Analytica Chimica Acta 1195 (2022) 339456

Contents lists available at ScienceDirect

Analytica Chimica Acta

journal homepage: www.elsevier.com/locate/aca

A label-free photoelectrochemical biosensor with ultra-low-background noise for lead ion assay based on the Cu_2O-CuO-TiO_2 heterojunction

Qiong Yu [1], Yamin Fu [1], Ke Xiao , Xiaohua Zhang , Cuicui Du , Jinhua Chen [*]

State Key Laboratory of Chemo/Biosensing and Chemometrics, College of Chemistry and Chemical Engineering, Hunan University, Changsha, 410082, PR China

HIGHLIGHTS

- A label-free PEC biosensor with ultra-low-background noise for Pb^{2+} assay.
- Pb^{2+}-assisted cyclic amplification strategy for the enhancement of PEC signal.
- Cu_2O-CuO-TiO_2 heterojunction as phosphate group recognition material and photoactive material.

GRAPHICAL ABSTRACT

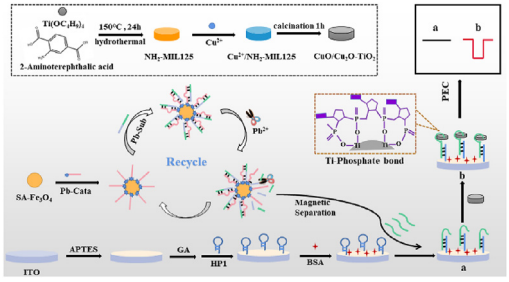

ARTICLE INFO

Article history:
Received 12 November 2021
Received in revised form
5 January 2022
Accepted 5 January 2022
Available online 7 January 2022

Keywords:
Photoelectrochemical biosensor
Cu_2O-CuO-TiO_2
Pb^{2+} assay
Label free
Ultra-low-background noise

ABSTRACT

Herein, a label-free and ultra-low-background-noise PEC biosensor was developed for lead ion (Pb^{2+}) assay based on the Cu_2O-CuO-TiO_2 heterojunction. By calcination of cupric ion (Cu^{2+}) doped-titanium based metal organic framework (MOF) material (NH_2-MIL-125), the Cu_2O-CuO-TiO_2 heterojunction was synthesized. With Pb^{2+}, lots of DNA single strands (S1) could be released based on the Pb^{2+} assisted cyclic amplification strategy and hybridized with hairpin DNA (HP1) on the modified electrode. The exposed phosphate groups on S1 can adsorb Cu_2O-CuO-TiO_2 heterojunction, which results in a large cathode photocurrent. Due to the good photoelectric property of Cu_2O-CuO-TiO_2 and Pb^{2+}-triggering cyclic amplification strategy, the constructed PEC biosensor achieves a wide linear detection range (10 fM - 1 μM) and a low detection limit (6.8 fM), which provides potential applications in ultrasensitive determination of Pb^{2+} in environmental water samples and organisms.

1. Introduction

Nowadays, water pollution has become one of the most urgent problems in the world. With the increase of industrial, agricultural and domestic wastewater discharge, the risk of human exposure to heavy metals is also increased [1]. As one of the most dangerous heavy metals [2], lead ions (Pb^{2+}) in trace concentration also pose a serious threat to organisms and human health. On account of the strong toxicity [3] and non-degradability [4] of Pb^{2+}, it is continuously accumulated through the food chain cycle of the ecosystem, resulting in irreversible damage to the human brain, kidney and nervous system [5]. Hence, it is tremendous practical significance to develop a sensitive and simple method to detect it. To date, various

* Corresponding author.
E-mail address: chenjinhua@hnu.edu.cn (J. Chen).
[1] Qing Yu and Yamin Fu contributed equally to this work.

https://doi.org/10.1016/j.aca.2022.339456
0003-2670/

assays have been developed for the determination of Pb^{2+}, including UV–vis spectroscopy [6], atomic absorption spectrometry [7], and inductively coupled plasma mass spectrometry, etc. [8] However, due to the limitations of large instrument and cumbersome operation, these traditional methods are generally only suitable for laboratory detection and not suitable for field analysis and daily testing. In order to solve these problems, in recent years, some promising Pb^{2+} detection methods have been developed, such as fluorescence spectrometry [9,10], electrochemistry [11–13], electrochemiluminescence [14,15], and colorimetry [16,17], etc. Although these technologies showed good performance for the detection of Pb^{2+}, some limitations including low selectivity, high background signal, and high measurement cost also existed [18]. Therefore, it is still a challenge to design a new method to detect Pb^{2+}.

Photoelectrochemical (PEC) biosensors are considered to be a kind of analysis technology with vigorous development and application prospects due to the separation of excitation light and detection signal, resulting in a low background noise [19–21]. Meanwhile, it also has the characteristics of miniaturization, low cost and easy operation, etc. [22] Recently, plenty of PEC biosensors have been constructed for the detection of Pb^{2+}. For example, Huang et al. proposed a "signal-on" PEC sensing platform for highly sensitive detection of Pb^{2+} by embedding methylene blue into 3D DNA to sensitize the substrate material [5]. Shi et al. prepared an ultrasensitive PEC aptasensor for Pb^{2+} assay based on the MoS_2-CdS:Mn nanocomposites and CdTe quantum dots [3]. Li et al. established a new-type PEC method for the detection of Pb^{2+} based on a dual-signal amplification strategy [23]. For above methods, the direct introduction of the photoelectric material on the electrode will produce a certain amount of initial photocurrent, and this background signal will limit the sensitivity. Therefore, it is worth exploring to design and develop a kind of PEC biosensor without background noise or with ultra-low background noise for the sensitive detection of Pb^{2+}.

For ultra-low-background-noise PEC sensor, the photoactive material is of vital importance to its performance. Titanium dioxide (TiO_2) has been widely studied in the fields of photocatalysis and solar cells because of its favorable valence band position, non-toxicity, chemical stability, light corrosion resistance and low cost, which is considered to be one of the most potential materials [24–26]. In addition, it is reported that the phosphate groups on ssDNA have a strong affinity to TiO_2 and it can selectively adsorb TiO_2 through the chelation interaction between phosphate groups and Ti ion [19]. However, the shortcomings of TiO_2 such as low surface area, rapid recombination of photo-generated electrons and holes, and wide band gap would limit the application of TiO_2 in the field of PEC biosensor. To solve these shortcomings, many researchers employed precious metals [27], dye or narrow-band-gap semiconductors (CdS, CdSe…) to sensitize TiO_2 [28,29]. But the scarcity of precious metals, the complex operation of dye sensitization process, and the great environmental pollution caused by heavy-metal-based semiconductor will limit its practical application.

It is reported that CuO and Cu_2O have the merits of low cost, hypotoxicity, abundance and the high photoelectric conversion efficiency [30]. Herein, we used the titanium based metal organic framework (MOF) material (NH_2-MIL-125) as the template due to its large surface area and porosity. Then Cu^{2+} was introduced into the surface and pores of NH_2-MIL-125 due to the chelation between Cu^{2+} and amino groups of NH_2-MIL-125. And the Cu_2O-CuO-TiO_2 heterojunction was synthesized by calcination of Cu^{2+}/NH_2-MIL-125. On account of the good photoelectric property of Cu_2O-CuO-TiO_2, a label-free and ultra-low-background-noise PEC biosensing platform was developed for the determination of Pb^{2+}. As depicted in Scheme 1, the hairpin DNA (HP1) was fixed on the 3-(aminopropyl)triethoxysilane-functionalized indium-tin oxide (APTES/ITO) electrode by glutaraldehyde (GA) cross-linking method. In the presence of Pb^{2+}, the Pb^{2+}-substrate strand (Pb-Sub) could be cleaved and would output lots of DNA single strands (S1), and S1 could hybridize with HP1 on the electrode. The exposed phosphate groups on S1 could adsorb Cu_2O-CuO-TiO_2 and a large cathode photocurrent was observed. Thus, Pb^{2+} was detected sensitively. The developed PEC biosensing platform provides a potential application prospect for real-time and rapid determination of Pb^{2+} in environmental water samples and organisms.

2. Experimental section

2.1. Preparation of Cu_2O-CuO-TiO_2 heterojunction

The Cu^{2+}-doped NH_2-MIL-125 was prepared based on the reported literature after a slight modification [31]. 0.52 mL of $Ti(OC_4H_9)_4$ and 1.087 g of 2-aminoterephthalic acid (NH_2-BDC) were dissolved in a mixed solution (CH_3OH: 2.7 mL; DMF: 24.3 mL). Then, the obtained mixture was fleetly stirred for 30 min. Next, the mixture was heated at 150 °C and maintained for 24 h in a Teflon-lined autoclave. After cooling down, the precipitate (NH_2-MIL-125) was obtained by centrifugation, washed and dried in vacuum at 60 °C. Sequentially, 50 mg of NH_2-MIL-125 powder and $Cu(NO_3)_2 \cdot 3H_2O$ with different mass were dispersed in 10 mL ultrapure water under ultrasonic stirring for 1 h. Then, the mixture was freeze-dried for 12 h to obtain the Cu^{2+}-doped NH_2-MIL-125 (called Cu^{2+}/NH_2-MIL-125). In order to completely convert NH_2-MIL-125 (Ti) precursor to TiO_2 without obvious change of its morphology [32] and to simultaneously produce CuO and Cu_2O [30], the Cu^{2+}/NH_2-MIL-125 was calcined in air at 350 °C for 1 h with the heating rate of 5 °C/min. Finally, the Cu_2O-CuO-TiO_2 heterojunction was obtained. The pure TiO_2 was prepared by the same procedure without Cu^{2+}.

2.2. Pb^{2+}-assisted recycling

10 μL (5 μM) of Pb^{2+}-catalysis strand (Pb-Cata, biotin-labeled) was added into 10 μL (5 μM) streptavidin-functionalized magnetic beads (SA-Fe_3O_4) suspension and stirred at 37 °C for 1 h. The Pb-Cata can be connected to SA-Fe_3O_4 through the specific binding between biotin and streptavidin. Subsequently, it was washed with Tri-HCl (10 mM, pH 7.4) for three times to eliminate excess Pb-Cata. After that, 10 μL of Pb-Sub (5 μM) was injected to the above mixture and maintained for 2 h at 37 °C. Thereafter, the various concentrations of Pb^{2+} was injected into above mixture and incubated for 2 h. Since the Pb^{2+} could specially cleave the corresponding binding site of Pb-Sub, the S1 related to target (Pb^{2+}) could be acquired by magnetic separation.

2.3. Fabrication of the PEC biosensor

The cleaned ITO slices were obtained according to the previous literature [33], and then treated with 2% APTES ethanol solution for 2 h and dried at 75 °C to obtain the amino-modified ITO electrode. Next, the GA (20 μL, 5 wt %) aqueous solution, as a crosslinking agent, was added onto the ITO/APTES for 2 h. Before using, the HP1 was denatured at 95 °C and maintained for 5 min. After cooling down to the room temperature, 20 μL of HP1 (1 μM) was added onto the electrode and incubated for 2 h to acquire the ITO/APTES/HP1 electrode. Then, it was soaked into 1 wt % of BSA solution to block the nonspecific sites. Afterwards, 20 μL of S1 solution was coated onto the ITO/APTES/HP1/BSA electrode and incubated for 2 h (37 °C). In the end, 20 μL of Cu_2O-CuO-TiO_2 (2 mg/mL)

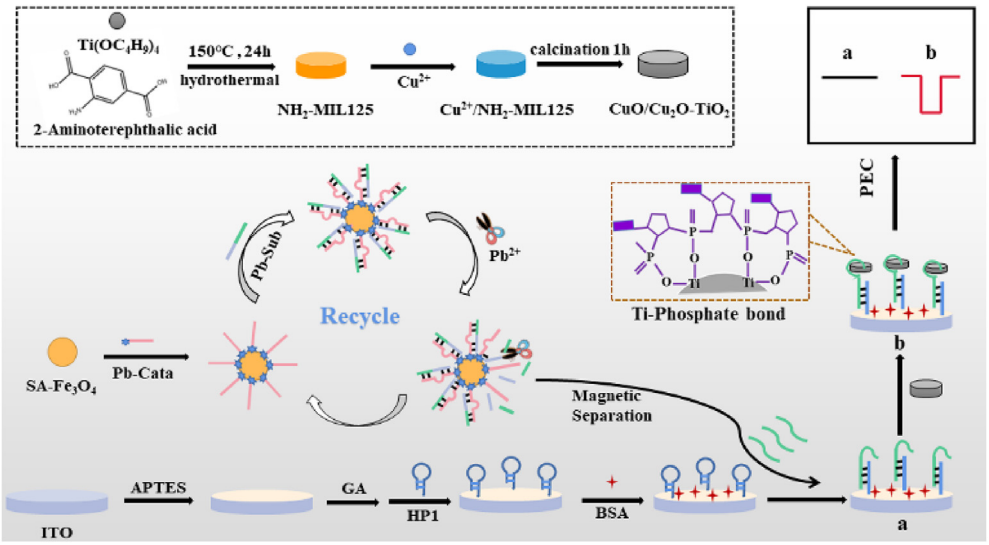

Scheme 1. Schematic illustration of the PEC biosensor for the detection of Pb^{2+}.

suspension was added on the ITO/APTES/HP1/BSA/S1 electrode at 37 °C for 2 h. After washing, the PEC test was carried out in Tris-HCl buffer (10 mM, pH 7.4) at −0.3 V.

3. Results and discussion

3.1. Characterization of materials

The morphologies of NH_2-MIL-125 and Cu_2O-CuO-TiO_2 heterojunction were characterized by scanning electron microscopy (SEM). From Fig. 1A, a disk-like morphology is showed in the SEM image of NH_2-MIL-125. After calcination of the Cu^{2+}-doped NH_2-MIL-125, the Cu_2O-CuO-TiO_2 heterojunction maintains the same shape of NH_2-MIL-125 (Fig. 1B) due to that the calcination temperature is lower than the skeleton decomposition temperature of NH_2-MIL-125 [32,34,35]. The TEM image (Cu_2O-CuO-TiO_2) is displayed in the inset of Fig. 1C and a rounded shape is consistent with the SEM image. At the same time, the spacing of lattice fringes in HRTEM image (Fig. 1C) are 0.275 nm and 0.247 nm, which are correspond to the CuO (110) and Cu_2O (111), implying that the composite includes CuO and Cu_2O. Here, the production of Cu_2O may result from the reduction of Cu^{2+} to Cu^{+} by reducing gases which are produced by insufficient combustion of organic ligands in the Cu^{2+}-doped NH_2-MIL-125 [30,36]. To confirm the element distribution of the prepared heterojunction, the element mapping is also provided in Fig. 1D. It is found that Ti, Cu and O elements are distributed uniformly in the Cu_2O-CuO-TiO_2 heterojunction.

The phase compositions of NH_2-MIL-125 and Cu_2O-CuO-TiO_2 were studied by X-ray diffraction (XRD). Fig. S1A (see supporting information section) is the XRD pattern of NH_2-MIL-125, which is consistent with that in the published literature, demonstrating a successful preparation of NH_2-MIL-125 [37]. The XRD patterns of Cu_2O-CuO-TiO_2 and pure TiO_2 are shown in Fig. S1B (see supporting information section). From the XRD curve of TiO_2, it is noted that the obtained TiO_2 by this pyrolysis temperature is amorphous phase, which is consistent with the previous report [37]. Simultaneously, the diffraction peaks of Cu_2O-CuO-TiO_2 are consistent with the standard phase card of CuO (PDF 80-1917), indicating CuO is present in the composite. But no diffraction peak of Cu_2O can be observed, which may be the low content of Cu_2O in the Cu_2O-CuO-TiO_2 heterojunction.

X-ray photoelectron spectroscopy (XPS) was further utilized to study the elemental valence state and composition of the Cu_2O-CuO-TiO_2 heterojunction. Fig. 2A clearly shows that the Ti, Cu and O elements are included in the Cu_2O-CuO-TiO_2 heterojunction. Fig. 2B shows that the peak value of Ti $2p_{3/2}$ is 458.8 eV, indicates that the valence of titanium is positive tetravalent [38]. And the two main peaks at 953.7 eV and 934.0 eV in Fig. 2C are corresponded to Cu $2p_{1/2}$ and Cu $2p_{3/2}$ peaks, respectively [30]. Furthermore, the peak of Cu $2p_{3/2}$ was separated into two peaks at 934.3 eV and 933.0 eV, which are associated with Cu^{2+} and Cu^{+} respectively. The presence of Cu^{+} confirms that the Cu_2O exists in the prepared material, which is consistent with the HRTEM result. Moreover, based on the electron oscillation, satellite peaks in the Cu 2p spectrum appear. From Fig. 2D, three peaks can be seen in the O 1s spectrum, which are oxygen vacancy (O_V), lattice oxygen (O_L) and adsorbed oxygen (O_C), respectively. And the presences of O_V and O_C are due to the chemisorption and dissociation of oxygen species (OH^-、O^- or O^{2-}). According to the above results, the Cu_2O-CuO-TiO_2 heterojunction is synthesized successfully.

Fig. 3A shows the nitrogen adsorption-desorption isotherm of the Cu_2O-CuO-TiO_2, and the calculated Brunauer Emmett Teller (BET) surface area is 75.1 m^2/g. From the insert plot in Fig. 3A, the pore size distribution curve displays that the prepared material has porous structure, and 18.4 nm of average pore size is obtained. Porous structure and large specific surface area are conducive to the absorption of excitation light source and electron transfer, which are benefit for the PEC process. From the UV−vis absorption spectra (Fig. 3B), the Cu_2O-CuO-TiO_2 displays a wider absorption range in the absorption region of visible light compared with the pure TiO_2, indicating that the Cu_2O-CuO-TiO_2 may have a good photoelectric property.

3.2. Electrochemical and photoelectrochemical characterization

Electrochemical impedance spectroscopy (EIS), as an effective method, was used to investigate each process of step-by-step modification of the ITO electrode. The electron transfer resistance (R_{ct}) is corresponding to the semicircle diameter in Nyquist diagram [39]. As shown in Fig. 4A, a small semicircle diameter (20.3 Ω, curve a) is obtained on the bare ITO electrode, indicating that it possesses a small electron transfer resistance. Subsequently, after modified with APTES and GA, the resistance value of R_{ct} increases to 46.7 Ω (curve b). Then, the modification of HP1 on the electrode through amide bond makes the R_{ct} value increase (116.8 Ω, curve c),

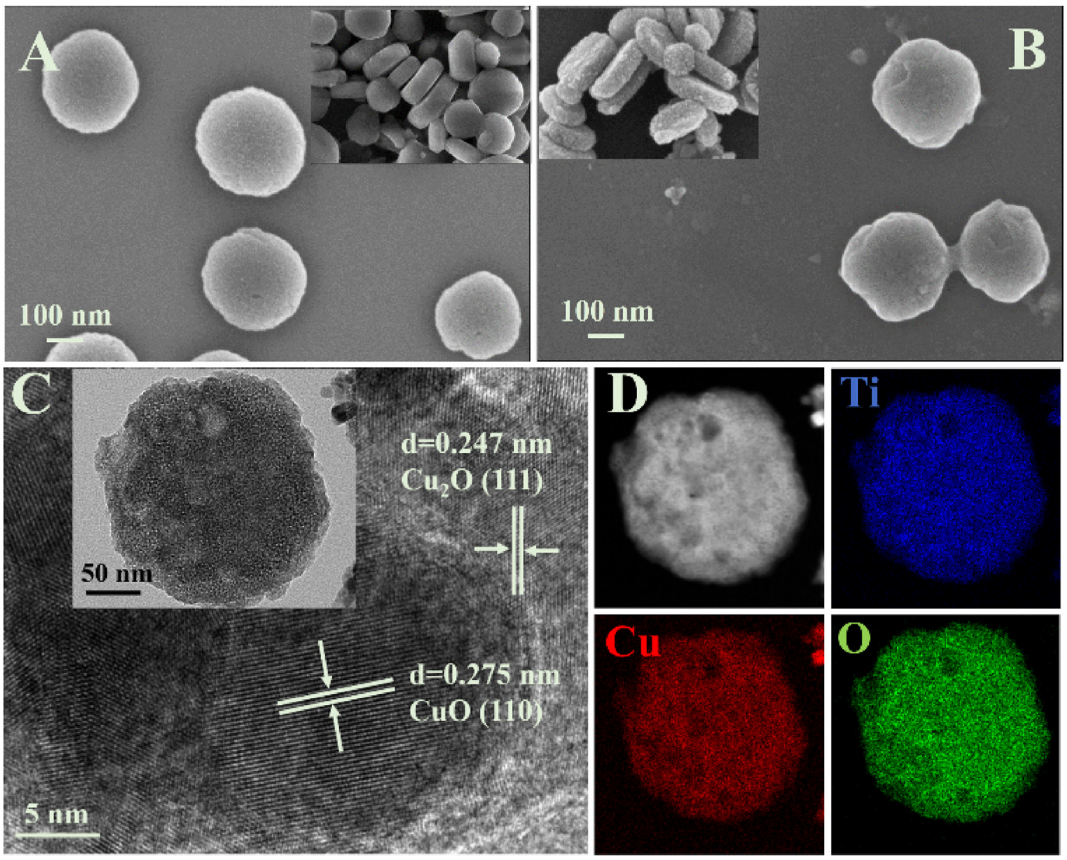

Fig. 1. SEM images of NH_2-MIL-125 (A) and Cu_2O-CuO-TiO_2 (B); (C) HRTEM image of the Cu_2O-CuO-TiO_2. (D) EDS mapping results of Cu_2O-CuO-TiO_2.

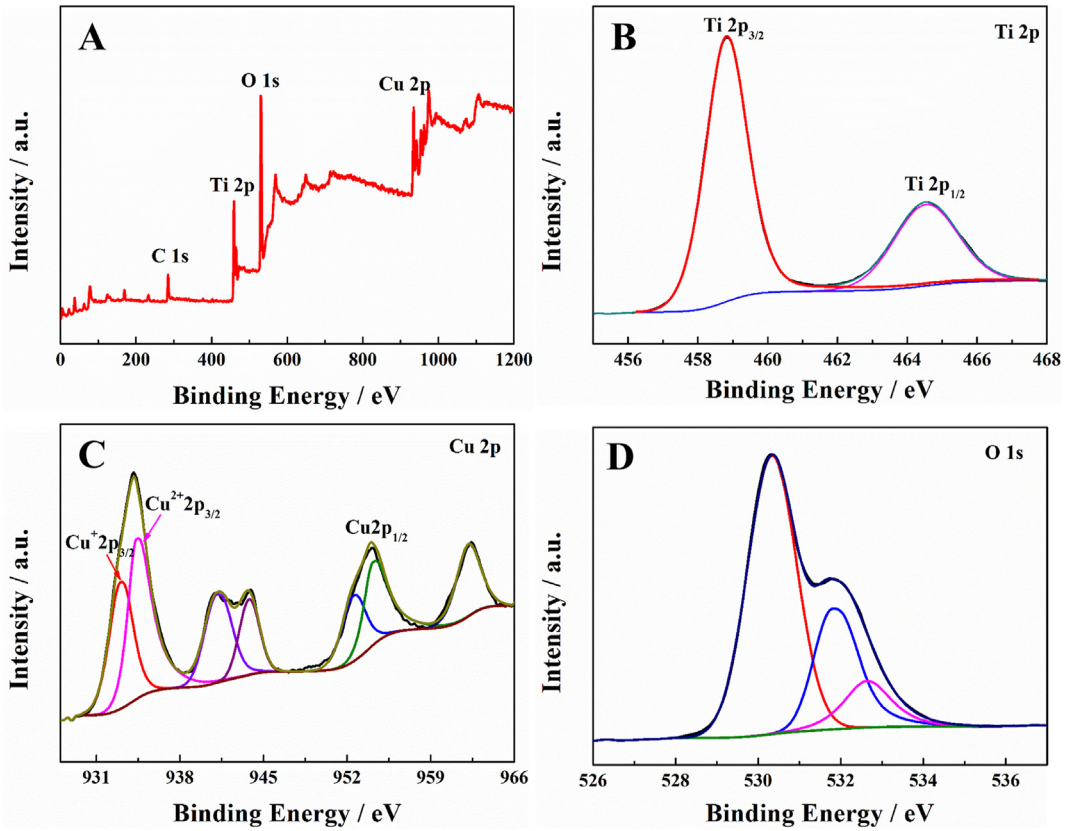

Fig. 2. (A) XPS spectrum of the Cu_2O-CuO-TiO_2. High-resolution XPS spectra of Ti 2p (B), Cu 2p (C) and O 1s (D).

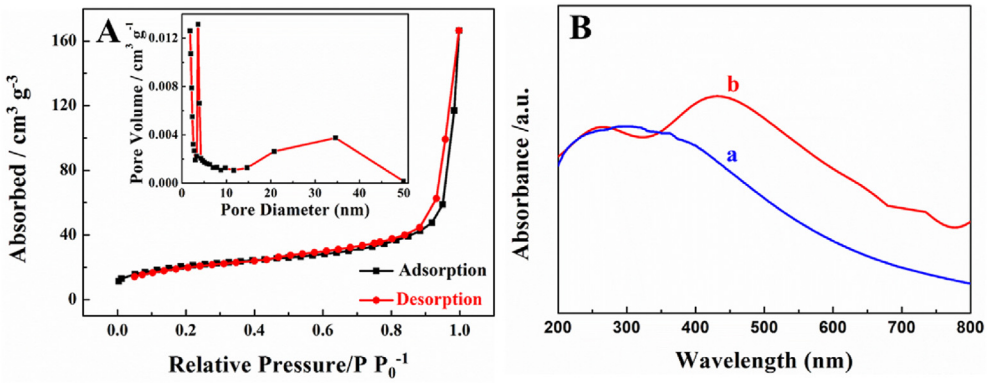

Fig. 3. (A) Nitrogen adsorption-desorption isotherms of the Cu_2O-CuO-TiO_2. (B) UV−vis absorption spectra of the TiO_2 (a) and Cu_2O-CuO-TiO_2 (b).

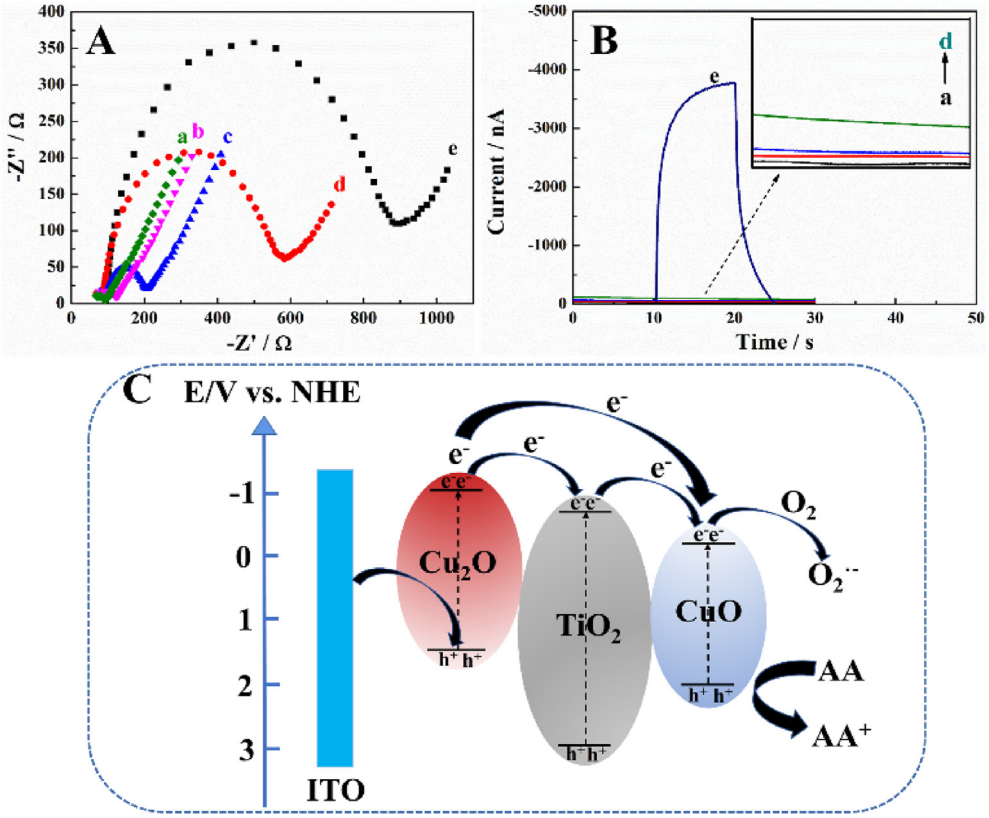

Fig. 4. (A) Nyquist plots in 5 mM $[Fe(CN)_6]^{3-/4-}$ containing 0.1 M KCl at open circuit potential (frequency range, 0.1−10^5 Hz). (B) Photocurrent responses in Tris-HCl (10 mM, pH 7.4) at −0.3 V. (a) bare ITO; (b) ITO/APTES; (c) ITO/APTES/HP1; (d) ITO/APTES/HP1/S1; (e) ITO/APTES/HP1/S1/Cu_2O-CuO-TiO_2. (C) PEC mechanism of ITO/Cu_2O-CuO-TiO_2 electrode.

which results from the blocking effect of HP1 on the $[Fe(CN)_6]^{3-/4-}$ transfer to the electrode surface. After blocking with BSA and then modifying with S1, the R_{ct} value increases significantly due to the non-conductive protein and negative-charged DNA molecules (511.0 Ω, curve d). Owing to the unfolding of hairpin structure, the phosphate radicals on the DNA molecules will be exposed. And after treated with Cu_2O-CuO-TiO_2 (curve e), the R_{ct} value increases to 774.6 Ω because of the introduction of the semiconductor material on the electrode via the chelation interaction between phosphate groups and Ti ion. Above results confirm that the PEC biosensor is prepared successfully according to Scheme 1.

Meanwhile, the construction process was also characterized by PEC method. As shown in Fig. 4B, no obvious photocurrents can be observed at the bare ITO, ITO/APTES, ITO/APTES/HP1 and ITO/APTES/HP1/S1 electrodes (curves a to d). After incubating the ITO/APTES/HP1/S1 electrode with Cu_2O-CuO-TiO_2, an obvious cathodic photocurrent generates, indicating that the Cu_2O-CuO-TiO_2 heterojunction is successfully introduced to the electrode through the specific affinity between TiO_2 and phosphate groups on S1 molecules. These results show that the prepared PEC biosensor displays an ultra-low-background noise for Pb^{2+} detection.

According to the valence band (VB) and conduction band (CB) values of Cu_2O, CuO [30] and TiO_2 [40], the possible electron transfer mechanism of the prepared biosensor may be as follows (Fig. 4C): The holes and electrons of the semiconductor materials are excited to the corresponding VB and CB under visible light. The electrons on the CB of Cu_2O transfer to the CB of TiO_2, and then to the CB of CuO. Subsequently, the electrons on the CB of CuO are

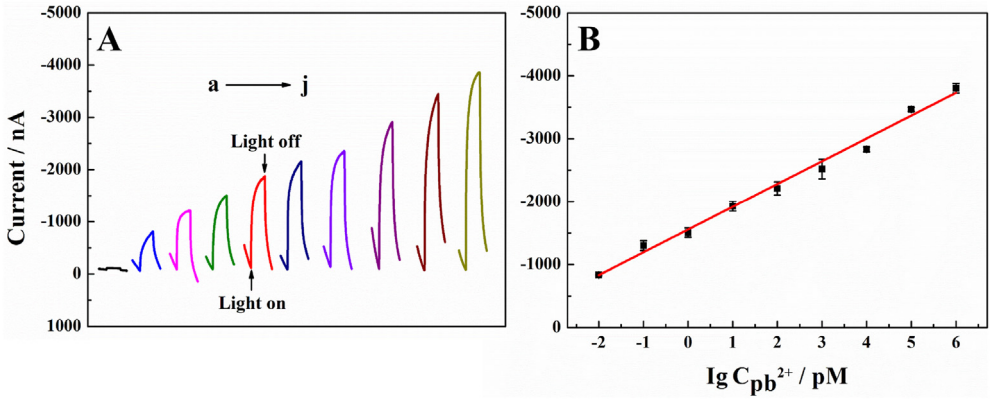

Fig. 5. (A) Photocurrent responses with different concentrations of Pb^{2+}. The concentrations (from a to j) are 0, 0.01, 0.1, 1, 10, 100, 1000, 10000, 100000, and 1000000 pM. (B) The linear calibration curve of the developed PEC biosensor for the detection of Pb^{2+}.

consumed by O_2 in the buffer solution. On the other hand, the generated holes are reduced by ascorbic acid (AA). Because of the matched energy levels of Cu_2O, CuO and TiO_2 can inhibit the recombination of the photo-generated electron/hole pairs, thus a significant cathode photocurrent can be observed.

3.3. Conditions optimization

Experimental condition optimization was carried out to get the good performance of the developed biosensor for Pb^{2+} assay. For PEC biosensor, the photoactive material plays a significant role. Fig. S2A (see supporting information section) shows the effect of different mass ratio between $Cu(NO_3)\cdot 3H_2O$ and NH_2-MIL-125 on the photocurrent of the developed PEC biosensor. It is noted that a maximal photocurrent is observed at the 60% mass ratio, and the photocurrent decreases when the mass ratio is more than 60%. The reason may be as follows: the appropriate amount of CuO in the Cu_2O-CuO-TiO_2 heterojunction can inhibit the recombination of electron/hole pairs and reduce the band gap of TiO_2. However, the excessive loading of CuO will block the active sites of TiO_2, resulting in the decrease of the photocurrent [41,42]. Therefore, 60% is selected as the optimal mass ratio between $Cu(NO_3)\cdot 3H_2O$ and NH_2-MIL-125 for the synthesis of the Cu_2O-CuO-TiO_2.

The Pb^{2+} cleavage time is another vital factor to affect the PEC signal of the prepared sensor. As shown in Fig. S2B (see supporting information section), the photocurrent increases when the cleavage time of Pb^{2+} increases. As the cleavage time is 60 min, the photocurrent reaches a platform. This shows that the appropriate cleavage time of Pb^{2+} is 60 min.

In addition, the incubating time of Cu_2O-CuO-TiO_2 will directly affect the photoelectric response of the PEC sensor, which is further optimized. According to Fig. S2C (see supporting information section), the photocurrent increases with the extended incubating time of Cu_2O-CuO-TiO_2. When the incubating time is 120 min, the PEC response reaches to a plateau, indicating that the optimal incubating time of Cu_2O-CuO-TiO_2 is 120 min.

3.4. Pb^{2+} assay

Under optimal conditions, the developed PEC biosensor is used for quantitative detection of Pb^{2+} concentration. Fig. 5A represents the PEC responses to the different concentrations of Pb^{2+} under the visible light excitation. It is found that the photocurrent response increases with the increasing of Pb^{2+} concentration in the range from 10 fM to 1 μM. Fig. 5B exhibits the linear relationship between the photocurrents and logarithmic (lg) concentrations of Pb^{2+} and the linear regression equation is $I\ (nA) = -3.62 \times 10^2 lgC_{Pb}^{2+} - 1.56 \times 10^3$ ($R^2 = 0.996$) with a limit of detection (LOD) of 6.8 fM (S/N = 3). By comparison, the developed PEC biosensors shows a lower detection limit and a wider linear response range than other previously reported works (Table 1).

3.5. Selectivity, reproducibility and stability

In order to verify the feasibility of the proposed PEC biosensor in practical application, selectivity and stability need to be explored. The selectivity test was carried out by adding 100-fold interfering substances relative to the concentration of Pb^{2+} (1 μM), including Cd^{2+}, Mg^{2+}, Ca^{2+} and Cu^{2+} (the concentration of all the interferences is 100 μM). As shown in Fig. 6A, the photocurrents for Pb^{2+} group and the mixture are much larger than that for the blank group and other interfering substances, indicating a good selectivity toward Pb^{2+} assay. On the other hand, the photocurrent obtained from five PEC biosensors are almost same (Fig. 6B), indicating the satisfactory repeatability of this biosensor. Furthermore, the stability of the electrode was also investigated. After storing in the refrigerator at 4 °C for 3 weeks, the developed PEC biosensor remains 92.8% of its initial photocurrent for Pb^{2+} assay. Which indicates that the prepared PEC biosensor get an acceptable stability.

3.6. Recovery test

In order to evaluate the practicability of the prepared PEC biosensor, a complex system of natural water samples was used and the recovery tests of Pb^{2+} were carried out. The water samples were

Table 1
Comparison of various methods for Pb^{2+} assay.

Methods	LOD (μM)	Linear range (μM)	Reference
fluorescence	0.01	0.01–0.1	9
fluorescence	1×10^{-3}	5.0×10^{-3}-1	10
electrochemistry	1.45×10^{-4}	4.8×10^{-4}-4.8	12
electrochemistry	7.68×10^{-4}	2×10^{-3}-0.24	13
electrochemiluminescence	6.4×10^{-6}	1×10^{-5}-0.1	14
electrochemiluminescence	3×10^{-6}	1×10^{-5}-2	15
colorimetry	0.025	0.05–1	16
colorimetry	0.032	0.1–10	17
photoelectrochemistry	1.67×10^{-8}	5.0×10^{-8}-0.1	3
photoelectrochemistry	3×10^{-8}	1×10^{-7}-1	5
photoelectrochemistry	3.16×10^{-6}	5.0×10^{-6}-1	23
photoelectrochemistry	**6.8×10^{-9}**	**1×10^{-8}-1**	**this work**

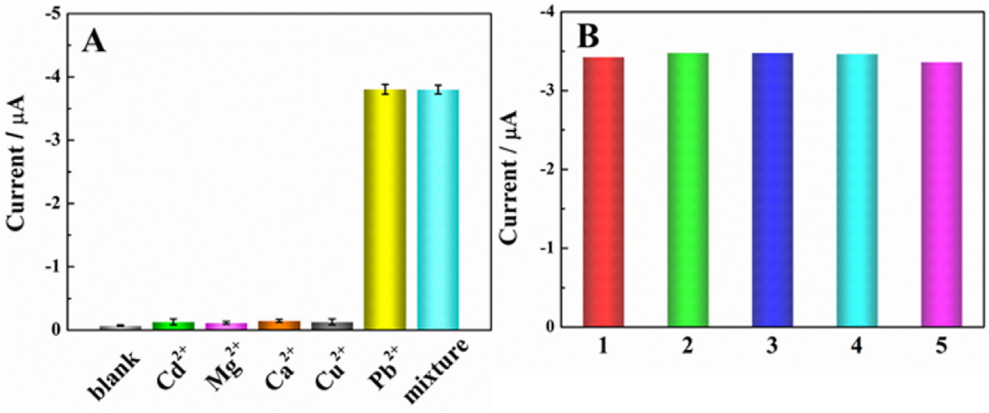

Fig. 6. (A) Selectivity of the developed PEC biosensor for Pb^{2+} assay. Pb^{2+} concentration, 1 μM; interferent concentration (Cd^{2+}, Mg^{2+}, Ca^{2+}, Cu^{2+}), 100 μM. (B) Repeatability of the PEC biosensor. Pb^{2+} concentration, 100 nM.

Table 2
Detection of Pb^{2+} in environmental water samples.

Sample	Add (nM)	Found (nM)[a]	RSD (%)	Recovery (%)
1	0.00	6.39	1.4	–
2	10.0	16.6	1.0	102
3	50.0	59.4	1.0	106
4	100	107	3.6	101

[a] Average value of three measurements.

obtained from the Xiangjiang river (Changsha, Hunan province, China). As shown in Table 2, 6.39 nM of Pb^{2+} can be found by using the developed PEC biosensor for the detection of water sample (Xiangjiang river), which is in good agreement with the result detected by inductively coupled plasma-mass spectrometry (6.76 nM, Table S2, see supporting information section), indicating that this PEC biosensor has a good veracity and practicability. After adding different concentrations of Pb^{2+} in the Xiangjiang water samples, and the recoveries for the added Pb^{2+} with 10.0 nM, 50.0 nM and 100 nM are 102%, 106%, and 101%, respectively. The above results demonstrate that the developed PEC biosensor has good applicability for Pb^{2+} assay in real samples.

4. Conclusions

In summary, based on the Cu_2O-CuO-TiO_2 heterojunction, the label-free PEC biosensing platform with ultra-low-background noise is prepared for the detection of Pb^{2+}. The proposed PEC biosensor exhibits a wide detection range (10 fM-1 μM) and low detection limit (6.8 fM) due to the good PEC performance of the Cu_2O-CuO-TiO_2 heterojunction originating from its large specific surface area and the formation of heterojunction. Moreover, this PEC biosensor possesses satisfactory reproducibility, good selectivity, acceptable stability, and good analytical applicability. The synthesized Cu_2O-CuO-TiO_2 heterojunction and the prepared PEC biosensor may have potential applications for the determination of Pb^{2+} in environmental water samples and organisms.

CRediT authorship contribution statement

Qiong Yu: Investigation, Methodology, Data curation, Writing – original draft. **Yamin Fu:** Methodology, Formal analysis, Datum analysis, Writing – review & editing. **Ke Xiao:** Writing – review & editing. **Xiaohua Zhang:** Validation, Data curation. **Cuicui Du:** Writing – review & editing. **Jinhua Chen:** Conceptualization, Supervision, Writing – review & editing.

Declaration of competing interest

The authors declare that they have no known competing financial interests or personal relationships that could have appeared to influence the work reported in this paper.

Acknowledgements

This work was financially supported by NSFC (21727810, 22074033).

Appendix A. Supplementary data

Supplementary data to this article can be found online at https://doi.org/10.1016/j.aca.2022.339456.

References

[1] S. Zhang, Z. Zhang, T. Wang, D. Zhang, X. Li, Z. Xue, D. Shan, X. Lu, High-throughput and ultratrace naked-eye colorimetric detection of Au^{3+} based on the gold amalgam-stimulated peroxidase mimetic activity in aqueous solutions, Chem. Commun. 53 (2017) 5056–5058.
[2] X. Zhang, W. Liu, X. Li, Z. Zhang, D. Shan, H. Xia, S. Zhang, X. Lu, Ultrahigh selective colorimetric quantification of chromium (VI) ions based on gold amalgam catalyst oxidoreductase-like activity in water, Anal. Chem. 90 (2018) 14309–14315.
[3] J.J. Shi, J.C. Zhu, M. Zhao, Y. Wang, P. Yang, J. He, Ultrasensitive photoelectrochemical aptasensor for lead ion detection based on sensitization effect of CdTe QDs on MoS_2-CdS:Mn nanocomposites by the formation of G-quadruplex structure, Talanta 183 (2018) 237–244.
[4] Z. Huang, J. Chen, Z. Luo, X. Wang, Y. Duan, Label-free and enzyme-free colorimetric detection of Pb^{2+} based on RNA cleavage and annealing-accelerated hybridization chain reaction, Anal. Chem. 91 (2019) 4806–4813.
[5] L.J. Huang, L. Yang, C.C. Zhu, H.M. Deng, G.P. Liu, Y.L. Yuan, Methylene blue sensitized photoelectrochemical biosensor with 3,4,9,10-Perylene tetracarboxylic acid film as photoelectric material for highly sensitive Pb^{2+} detection, Sens. Actuators, B 274 (2018) 458–463.
[6] Q. Hu, G. Yang, Y. Zhao, J. Yin, Determination of copper, nickel, cobalt, silver, lead, cadmium, and mercury ions in water by solid-phase extraction and the RP-HPLC with UV-Vis detection, Anal. Bioanal. Chem. 375 (2003) 831–835.
[7] I. Narin, M. Soylak, L. Elci, M. Dogan, Determination of trace metal ions by AAS in natural water samples after preconcentration of pyrocatechol violet complexes on an activated carbon column, Talanta 52 (2000) 1041–1046.
[8] A. Griffiths, H. Packman, Y.L. Leung, B.J. Coles, K. Kreissig, S.H. Little, T. Flierdt, M. Rehkämper, Evaluation of optimized procedures for high-precision lead isotope analyses of seawater by multiple collector inductively coupled plasma mass spectrometry, Anal. Chem. 92 (2020) 11232–11241.
[9] L. Zhang, B. Han, T. Li, E. Wang, Label-free DNAzyme-based fluorescing molecular switch for sensitive and selective detection of lead ions, Chem. Commun. 47 (2011) 3099–3101.
[10] L. Guo, D. Nie, C. Qiu, Q. Zheng, H. Wu, P. Ye, Y. Hao, F.F. Fu, G. Chen, A G-quadruplex based label-free fluorescent biosensor for lead ion, Biosens. Bioelectron. 35 (2012) 123–127.
[11] X. Wang, C. Yang, S. Zhu, M. Yan, S. Ge, J. Yu, 3D origami electrochemical

device for sensitive Pb^{2+} testing based on DNA functionalized iron-porphyrinic metal-organic framework, Biosens. Bioelectron. 87 (2017) 108–115.
[12] G. Ran, F. Wu, X. Ni, X. Li, X. Li, D. Liu, Sun, J.C. Xie, D. Yao, W. Bai, A novel label-free electrochemical aptasensor with one-step assembly process for rapid detection of lead (II) ions, Sens. Actuators, B 320 (2020) 123–127.
[13] M.A. Mhammedi, M. Achak, A. Chtaini, $Ca_{10}(PO_4)_6(OH)_2$-modified carbon-paste electrode for the determination of trace lead (II) by square-wave voltammetry, J. Hazard Mater. 161 (2009) 55–61.
[14] Y.F. Wu, Z.M. Cai, G.H. Wu, M.C. Rong, Y.Q. Jiang, C.Y.J. Yang, X. Chen, A novel signal-on DNAzyme-based electrochemiluminescence, sensor for Pb^{2+}, Sens. Actuators, B 191 (2014) 60–66.
[15] Y. Zhang, J. Xu, S. Zhou, L. Zhu, X. Lv, J. Zhang, L. Zhang, P. Zhu, J. Yu, DNAzyme-Triggered visual and ratiometric electrochemiluminescence dual-readout assay for Pb(II) based on an assembled paper device, Anal. Chem. 92 (2020) 3874–3881.
[16] N. Ding, Q. Cao, H. Zhao, Y. Yang, L. Zeng, Y. He, K. Xiang, G. Wang, Colorimetric assay for determination of lead (II) based on its incorporation into gold nanoparticles during their synthesis, Sensors 10 (2010) 11144–11155.
[17] T. Li, E. Wang, S. Dong, Lead (II)-induced allosteric G-quadruplex DNAzyme as a colorimetric and chemiluminescence sensor for highly sensitive and selective Pb^{2+} detection, Anal. Chem. 82 (2010) 1515–1520.
[18] Y. Zang, J. Lei, Q. Hao, H. Ju, Signal-on" photoelectrochemical sensing strategy based on target-dependent aptamer conformational conversion for selective detection of lead(II) ion, ACS Appl. Mater. Interfaces 6 (2014) 15991–15997.
[19] Y. Fu, F. Ding, J. Chen, M. Liu, X. Zhang, C. Du, S. Si, Label-free and near-zero-background-noise photoelectrochemical assay of methyltransferase activity based on a Bi_2S_3/Ti_3C_2 Schottky junction, Chem. Commun. 56 (2020) 5799–5802.
[20] D. Dong, D. Zheng, F.Q. Wang, X.Q. Yang, N. Wang, G. Yuan, L.H. Guo, J. Cheng, Quantitative photoelectrochemical detection of biological affinity reaction: biotin-avidin interaction, Anal. Chem. 76 (2004) 499–501.
[21] Y. Zang, J. Lei, H. Ju, Principles and applications of photoelectrochemical sensing strategies based on biofunctionalized nanostructures, Biosens. Bioelectron. 96 (2017) 8–16.
[22] R. Wang, S. Chen, Y.H. Ng, Q. Gao, S. Yang, S. Zhang, F. Peng, Y. Fang, S. Zhang, ZnO/CdS/PbS nanotube arrays with multi-heterojunctions for efficient visible-light-driven photoelectrochemical hydrogen evolution, Chem. Eng. J. 362 (2019) 658–666.
[23] Y. Li, F. Chen, Z. Luan, X. Zhang, A versatile cathodic "signal-on" photoelectrochemical platform based on a dual-signal amplification strategy, Biosens. Bioelectron. 119 (2018) 63–69.
[24] D.B. Seo, S.S. Bae, E.T. Kim, Efficient visible-light photocatalysis of $TiO_{2-\delta}$ nanobelts utilizing self-induced defects and carbon doping, Nanomaterials 11 (2021) 1377.
[25] Y. Chen, Q. Tao, W. Fu, H. Yang, X. Zhou, S. Su, D. Ding, Y. Mu, X. Li, M. Li, Enhanced photoelectric performance of PbS/CdS quantum dot co-sensitized solar cells via hydrogenated TiO_2 nanorod arrays, Chem. Commun. 50 (2014) 9509–9512.
[26] A. Meng, L. Zhang, B. Cheng, J. Yu, Dual cocatalysts in TiO_2 photocatalysis, Adv. Mater. 31 (2019), 1807660.
[27] W. Guo, J. Wang, W. Guo, Q. Kang, F. Zhou, Interference-free photoelectrochemical immunoassays using carboxymethylated dextran-coated and gold-modified TiO_2 nanotube arrays, Anal. Bioanal. Chem. 413 (2021) 4847–4854.
[28] Y. Zang, R. Cao, C. Zhang, Q. Xu, Z. Yang, H. Xue, Y. Shen, TiO_2-sensitized double-shell ZnCdS hollow nanospheres for photoelectrochemical immunoassay of carcinoembryonic antigen coupled with hybridization chain reaction-dependent Cu^{2+} quenching, Biosens. Bioelectron. 185 (2021), 113251.
[29] Y.X. Dong, J.T. Cao, Y.M. Liu, S. Ma, A novel immunosensing platform for highly sensitive prostate specific antigen detection based on dual-quenching of photocurrent from CdSe sensitized TiO_2 electrode by gold nanoparticles decorated polydopamine nanospheres, Biosens. Bioelectron. 91 (2017) 246–252.
[30] Y. Fu, K. Zou, M. Liu, X. Zhang, C. Du, J. Chen, Highly selective and sensitive photoelectrochemical sensing platform for VEGF165 assay based on the switching of photocurrent polarity of CdS QDs by porous Cu_2O-CuO flower, Anal. Chem. 92 (2020) 1189–1196.
[31] D. Ao, J. Zhang, H. Liu, Visible-light-driven photocatalytic degradation of pollutants over Cu-doped NH_2-MIL-125(Ti), J. Photochem. Photobiol., A 364 (2018) 524–533.
[32] B. Yan, L. Zhang, Z. Tang, M. Al-Mamun, H. Zhao, Palladium-decorated hierarchical titania constructed from the metal-organic frameworks NH_2-MIL-125 (Ti) as a robust photocatalyst for hydrogen evolution, Appl. Catal., B 218 (2017) 743–750.
[33] R. Yang, K. Zou, Y. Li, L. Meng, X. Zhang, J. Chen, Co_3O_4-Au polyhedra: a multifunctional signal amplifier for sensitive photoelectrochemical assay, Anal. Chem. 90 (2018) 9480–9486.
[34] G. Mo, L. Wang, J. Luo, Controlled thermal treatment of NH_2-MIL-125 (Ti) for drastically enhanced photocatalytic reduction of Cr (VI), Separ. Purif. Technol. 277 (2021), 119643.
[35] M.Z. Hussain, M. Bahri, W.R. Heinz, Q. Jia, O. Ersen, T. Kratky, R.A. Fischer, Y. Zhu, Y. Xia, An in situ investigation of the thermal decomposition of metal-organic framework NH_2-MIL-125(Ti), Microporous Mesoporous Mater. 316 (2021), 110957.
[36] M.N. Shaikh, M.M. Abdelnaby, A.S. Hakeem, G.A. Nasser, Z.H. Yamani, Co_3O_4/nitrogen-doped graphitic carbon/Fe_3O_4 nanocomposites as reusable catalysts for hydrogenation of quinoline, cinnamaldehyde, and nitroarenes, ACS Appl. Nano Mater. 4 (2021) 3508–3518.
[37] S. Lv, Y. Tang, K. Zhang, D. Tang, Wet NH_3-triggered NH_2-MIL-125(Ti) structural switch for visible fluorescence immunoassay impregnated on paper, Anal. Chem. 90 (2018) 14121–14125.
[38] M. Stefik, F.J. Heiligtag, M. Niederberger, M. Grätzel, Improved nonaqueous synthesis of TiO_2 for dye-sensitized solar cells, ACS Nano 7 (2013) 8981–8989.
[39] A. Bardea, F. Patolsky, A. Dagan, I. Willner, Sensing and amplification of oligonucleotide-DNA interactions by means of impedance spectroscopy: a route to a Tay-Sachs sensor, Chem. Commun. (1999) 21–22.
[40] H. Li, J. Li, Y. Zhu, W. Xie, R. Shao, X. Yao, A. Gao, Y. Yin, Cd^{2+}-doped amorphous TiO_2 hollow spheres for robust and ultrasensitive photoelectrochemical sensing of hydrogen sulfide, Anal. Chem. 90 (2018) 5496–5502.
[41] Z. Zhang, X. Li, D. Guan, Y. Gao, J. Wu, Q. Liu, et al., Photocatalytic oxidation of gas-phase HgO by Fe-doped TiO_2 hollow microspheres, Mater. Lett. 291 (2021), 129538.
[42] W. Xu, H. Wang, X. Zhou, T. Zhu, CuO/TiO_2 catalysts for gas-phase HgO catalytic oxidation, Chem. Eng. J. 243 (2014) 380–385.